Super typhoon induced high silica export from Arakawa River, Japan

Super typhoon induced high silica export from Arakawa River, Japan

Atsushi Kubo[1*] and Natsuki Yamahira[1]

[1]Department of Geosciences, Shizuoka University, 856 Ohya, Suruga-ku, Shizuoka city, Shizuoka prefecture, 422-8529, Japan.

*Corresponding Author

Atsushi Kubo (kubo.atsushi@shizuoka.ac.jp, telephone: +81-54-238-4794)

Department of Geosciences, Shizuoka University, 856 Ohya, Suruga-ku, Shizuoka, 422-8529, Japan.

Type of Paper: Research Paper

Abstract

Dissolved silicate (DSi) and particulate silica (PSi) concentrations were measured at Arakawa River and at sewage treatment plants (STP) during October 2018 to October 2019. These included flooding observations after super Typhoon Hagibis. At ordinary water levels, the STP effluents were found to be the largest source of DSi in the river. Although DSi concentrations during the flooding events (165 μmol L^{-1}) decreased by about 25% compared to that of ordinary water level (221 μmol L^{-1}), PSi was more than sixteen times higher value (301 μmol L^{-1}) compared to that of ordinary water level (18 μmol L^{-1}). Loading amounts of DSi and PSi (±1 standard error) were 1.5×10^8 ($\pm 0.1 \times 10^8$) and 0.15×10^8 ($\pm 0.02 \times 10^8$) mol $year^{-1}$, respectively, excluding the data of Typhoon Hagibis. Loading amounts during flooding events of DSi and PSi were 1.2×10^8 ($\pm 0.1 \times 10^8$) and 2.4×10^8 ($\pm 0.4 \times 10^8$) mol $15days^{-1}$, respectively. Although the silica loading at ordinary water level was mainly derived from DSi, the silica loading during flooding events was extremely large due to both high level of DSi and PSi; moreover, it was higher than the annual loading amount.

Keywords: Dissolved silicate; particulate silica; flooding; runoff; sewage treatment plant

1. Introduction

Dissolved silicate (DSi) in water is an essential component for some aquatic plants and organisms. Primary production of diatoms accounts for about 45% of the primary production of the entire ocean (Nelson et al., 1995; Rousseaux and Gregg, 2014). Although DSi is naturally supplied to water by the weathering process, with aluminosilicates dissolved in rainwater, river water, groundwater, and seawater, human activity has also affected the silica cycle (Tréguer and de la Rocha, 2013). Dams act as one of the major sinks of DSi because they increase the water residence time, inducing diatom blooms and particulate silica (PSi) sedimentation (Wei et al., 2015; Yang et al., 2018; Maavara et al., 2020). In contrast, supply from farmland, groundwater, and sewage treatment plants (STP) is one of the sources of DSi (van Dokkum et al., 2004; Sferratore et al., 2006; Kumagai et al., 2011). Silicate fertilizers have been applied for a long time to stabilize rice yield, but fertilizer application rates have been decreasing since the 1970s in Japan (Furumai et al., 2012). DSi concentrations in groundwater is high because some coastal aquifers consist of aluminosilicates (e.g., Ragueneau et al., 2006). However, penetration of rainwater into groundwater was reduced significantly because roads, rivers, and waterways were covered by concrete along with coastal urbanization. Most of the rainwater flows through the ground surface and flows into STPs. As a result, direct discharge of groundwater into the river is small proportion of freshwater balance in highly urbanized coast area of Tokyo (Furumai, 2008). Although there were few research studies on the fluctuation of DSi by the sewage treatment process, Maguire and Fulweiler (2017) reported that the concentrations of DSi between inflow and effluent waters did not change significantly. In addition, the DSi concentration in river water increased after the inflow of STP effluents because groundwater which is higher concentration than river water is used as domestic water (Inoue and Akagi, 2006).

At present, there is concern about material cycling change derived from climate change in the ocean (Bindoff, in press). Extreme weather has increased due to increased seawater temperature, atmospheric heat, and water vapor (Staten et al., 2018; Chauvin et al., 2020). As a result, the outflow of river water is predicted to increase due to the increase in precipitation and typhoons (Scavia et al., 2002; Touma et al., 2019). Furthermore, if global warming continues, the westerly wind over Japan will move northward due to changes in the atmospheric circulation, resulting in the decrease of moving speed of the typhoon in recent decades (Yamaguchi et al., 2020). Therefore, the flooding event frequency and the scale may increase. However, few studies have been conducted on the fluctuations of DSi during flooding events, and it is difficult to predict future changes. Understanding the riverine silicon cycling with flooding event will help to project the potential influences of further riverine climate change in the future.

2. Study site and methods

The basin area of the Arakawa river is 2940 km^2 and the total length is 173 km. The land use of the basin is 43% forest, 28% urban area, and 7% paddy field (Nihei et al., 2007). Although the urban area is 28% of the basin, there are 24 STPs in the basin due to its population being 9.75 million. There are three dams in the upper stream of the Arakawa river, but it is not affected by domestic drainage. In the middle part, there are paddy fields spread throughout the watershed, with progressive urbanization. The downstream area is densely populated with urban areas, and a large amount of domestic wastewater flows in. Therefore, about half of the downstream river water is reported to be treated sewage water (Kubo et al., 2015; Kubo et al., 2017).

Observations were made every two months from October 2018 to October 2019. In October 2019, three samplings were conducted on October 12 and 13 (only station A25) and October 26 (all stations) after the flooding events. Sampling was performed at 10 stations from the upper stream to downstream (Figure 1). Single water samples were collected at the center of river channel from the bridge using the bucket. There is a dam between observation points A2 and A3. There are STPs between observation points A18 and A25, and the sewage treatment population is about 3.5 million, which is the largest in the Arakawa basin.

Water temperature and electrical conductivity were measured after collecting surface water by a bucket (EC300, YSI nanotech Inc., OH, USA). Then, the water was collected in 1L polycarbonate bottles. The collected samples were immediately filtered through a glass fiber filter (GF/F, pore size about 0.7 μm, Whatman, UK) and a nuclepore filter (PC MB, pore size 0.6 μm, Whatman, UK). The filtrate from a nuclepore filter was stored in a polypropylene tube (SARSTEDT, Germany) for analysis of DSi and phosphate. After filtering, the glass fiber filter was placed in a polypropylene tube (SARSTEDT, Germany) containing N,N-dimethylformamide for chlorophyll a (Chl *a*) measurement (Suzuki and Ishimaru, 1990); the nuclepore filter was placed in a polypropylene tube (SARSTEDT, Germany) for PSi analysis.

DSi and phosphate were measured within one month using the molybdenum blue method of Hansen and Koroleff (1999) and Murphy and Riley (1962), respectively, using a spectrophotometer with a syringe shipper unit (UVmini1240, Shimadzu, Japan). As DSi is known to form a polymer during freezing (MacDonald et al., 1986), the samples were defrosted with hot water at about 40 ºC, and then returned to room temperature before analysis. Samples frozen for one month have a minor DSi loss of up to only 1% (Becker et al., 2019). In addition, we compared the DSi concentrations of defrosted with hot water at 40 ºC for 3 hours, 50 ºC for 3 hours (Becker et al., 2019), and refrigerator for 4 days (Zhang and Ortner, 1998) after 10 days frozen. The DSi concentrations of defrosted with three method were not significantly different each other (two tailed t-test, $p>0.2$, $n=5$). PSi was measured by the alkali extraction method (Krausse et al., 1983; Ragueneau and Treguer, 1994; Hashihama, 2018). At first, the filter samples were dried at 60°C and 10 mL of 0.2 mol L^{-1} NaOH were added to the filter in the tube. The tubes were soaked in water bath at 100°C for 15 min. After cooling, 10 mL of 0.2 mol L^{-1} HCl were added. Finally, filter the solution with nuclepore filter to remove suspended matter and the concentrations were measured using the molybdenum blue method as with the same method of DSi. In this study, mineral silica and biogenic silica were not analyzed separately, so PSi was considered as the total amount of particulate silica. Chl *a* concentration was measured using a fluorometer (Trilogy, Turner Degins, Sunnyvale, CA, USA).

There is a correlation between discharge rate and water level in the Arakawa river (Tanaka et al., 2007). Therefore, the water level and discharge rate curve is created from the data on river water level and the discharge rate from January 1, 2015 to December 31, 2017 (Kanto Regional Development Bureau: https://www.ktr.mlit.go.jp/index.htm). This is because discharge rate during the observation periods were unpublished data. The created water level and discharge curve is, as follows:

$$D\ (m^3/s) = 80.7 \times [WL]^2 + 552.1 \times [WL] + 954.4 \quad (r^2 = 0.974) \qquad (1)$$

D means discharge rate ($m^3\ s^{-1}$) and WL indicates the water level (m) at the river. River discharge rate was calculated by substituting the water level data from October 1, 2018 to October 31, 2019 (Kanto Regional Development Bureau: https://www.ktr.mlit.go.jp/index.htm) into the above equation.

Loading amount of DSi, PSi, and phosphate during ordinary water level (365 days from October 1, 2018 to September 30, 2019) and flooding events (15 days from October 12, 2019 to October 26, 2019) were estimated using Beal's unbiased ratio estimator (Beale, 1962; Ricker, 1973; Dolan et al., 1981; Fulweiler and Nixon, 2005). This method is ideally suited to those situations where there is an abundance of flow information with respect to a tributary, but there is relatively little information on the concentration (Dolan et al., 1981; Richards and Holloway, 1987; Richards, 1999). The loading amount estimation is, as follows:

$$\mu_y = \mu_x \frac{m_y}{m_x}\left(\frac{1+\frac{1}{n}\frac{S_{xy}}{m_x m_y}}{1+\frac{1}{n}\frac{S_x^2}{m_x^2}}\right) \qquad (2)$$

$$S_{xy} = \frac{1}{(n-1)}\sum_{i=0}^{n} x_i y_i - n m_x m_y \qquad (3)$$

$$S_x^2 = \frac{1}{(n-1)}\sum_{i=0}^{n} x_i^2 - n m_x^2 \qquad (4)$$

where, μ_y means loading amount (mol year^{-1}), μ_x means averaged water discharge rate (m^3 s^{-1}), m_y means daily loading for days when concentrations were determined, m_x means daily discharge on those days when concentrations were determined. *n* means the number of samplings.

3. Results and Discussion

3.1 Spatial and temporal variations of DSi and PSi

Spatial and temporal variations of DSi and PSi concentrations at each station are shown in Figure 2 and Table S1. The concentration of DSi and PSi increased downstream. The highest concentrations of DSi and PSi were observed at station A18 and A25, respectively. At station A2 in the reservoir lake, DSi concentrations decrease from spring to summer. In contrast, PSi concentrations increase from spring to summer. From stations A3 to A9, the fluctuations were minimal and constant throughout the year. In contrast, the seasonal variations were large in the middle and lower river stations, but no clear seasonal change was observed. In the middle and downstream, PSi concentrations increased during spring and summer, and the variability was larger than in the upper stream. Although phosphate concentrations in the upper stream stations were lower than the detection limit, the concentration increased downstream (Figure 2). Highest concentration was observed at station A25. In the middle and downstream, phosphate concentrations decreased during summer and autumn.

At station 2, seasonal variation in DSi concentration shows an inverse correlation with that of PSi (R^2=0.70, p<0.05). As active photosynthesis occurred at the dam lakes, as reported by Maavara et al. (2020), DSi reduced. In contrast, Chl *a* and PSi increased. From station A3 to A5 downstream of the dam, the DSi concentration was higher than that of station A2. This is probably because DSi concentration increased again due to the release of PSi from the dam, leading to dissolution downstream. Furthermore, inflow from a tributary and/or groundwater with higher DSi concentration than dam lake water is considered. Therefore, the effect of DSi removal at the dam lake is a minor contribution to the middle and downstream.

Regardless of the observation months, DSi concentration increased in the middle river (station A17 and A18), which had the largest STP in the basin. River flow from the upper stream of Arakawa river and the STP effluent discharge from the basin was in the ratio of 1: 1 (Kubo et al., 2015; Kubo et al., 2017). Therefore, the average DSi concentrations at station A14 in the middle of the Arakawa river basin (134.3 ± 37.2 μmol L^{-1}), which is not affected by the STP effluent, is mixed with the STP effluent (291.0 ± 68.9 μmol L^{-1}) at a ratio of 1: 1. The mixed concentration is about 213 μmol L^{-1}, which is about the same concentration as the average DSi concentration at stations A17 (257.0 ± 39.5 μmol L^{-1}) and A18 (234.5 ± 49.7 μmol L^{-1}). Therefore, the large increase in DSi concentrations in the middle river was due to inflow of STP effluents. Direct inflow of groundwater to the river may have a great impact as a source of DSi to Arakawa river. Since there was no significant increase in DSi concentrations from the upper stream to the middle stream, the effect of direct groundwater discharge in the upper stream was small. On the other hand, increase of DSi and phosphate concentrations in the middle river (stations A17 and A18) could be direct discharge of groundwater. The concentrations of DSi in groundwater around the observation station (579 ± 174 μmol L^{-1}, n=12; Miyashita, 2004) were significantly higher than those in middle river water (246 ± 46 μmol L^{-1}) and STP effluent (291 ± 69 μmol L^{-1}). In contrast, phosphate concentrations in groundwater around the observation station (<1.0 μmol L^{-1}, n=12; Miyashita, 2004) were significantly lower than those in middle river water (5.0 ± 3.2 μmol L^{-1}) and STP effluent (12.4 ± 5.6 μmol L^{-1}). Therefore, the contribution ratio of the direct inflow of groundwater was likely low because phosphate concentrations as well as DSi concentrations was also increased in the downstream. However, there are few data on direct inflow of groundwater in Arakawa river, so further research is needed to quantify nutrient source to the river water.

The ratio of DSi/phosphate in the middle part of the river (St. 14; 205.2 ± 121.5), which was not affected by the STP effluent were much higher than that of STP effluent (27.5 ± 14.9). As a result, the ratio was greatly reduced in the downstream that was strongly affected by the inflow from the STP (St. 17, 18, and 25; 82.4 ± 64.8). The ratio of DSi/phosphate in STP effluent is dramatically different compared to the upper and middle stream water. Tokyo Bay which is the Arakawa river estuary was phosphorus depleted coastal area throughout the year and DSi depleted only spring (28.0 ± 23.9; Kubo et al., 2019). Therefore, if the inflow of STP effluent increases in the future, not only the phosphorus depletion but also the DSi depletion in Tokyo Bay may further accelerate.

3.2 Loading amount of silicon during flooding event

The average discharge rate of the Arakawa river from October 1, 2018 to September 30, 2019 was 24.2 m^3 s^{-1}; data of October 2019 was unavailable due to the super typhoon (Figure S1). Typhoon Hagibis (minimum pressure 915 hPa, maximum wind speed 55m s^{-1}), which occurred on the eastern part of the Mariana Islands on October 6, 2019 and landed on Japan on the October 12, 2019, caused heavy precipitation on the 11th. Precipitation from October 11th and 12th was 488 mm (JMA; http://www.jma.go.jp/jma/index.html). The discharge rate also increased immediately after Typhoon Hagibis and reached a maximum of 2162.6 m^3 s^{-1}. Immediately after Typhoon Hagibis, Typhoon Bualoi passed through the eastern part of Tokyo, also causing heavy rainfall. Precipitation at this time was 182 mm from October 18 to 25. The discharge rate increased again and reached a maximum of 735.8 m^3 s^{-1}.

On October 12 and 13, 2019, observations were conducted only at the station A25; on

October 26, observations were made at all stations. At station A25, DSi concentration on October 12, 13, and 26 was 174.5, 169.1 and 151.7 μmol L^{-1}, respectively, and PSi concentration was 394.1, 270.7 and 237.0 μmol L^{-1}, respectively (Table S2). The phosphate concentrations were 3.5, 2.0, and 1.8 μmol L^{-1}, respectively. Spatial variations of DSi, PSi, and phosphate on October 26, 2019 are presented in Figure 3. Large change in concentration was not observed from upper stream to downstream, unlike the ordinary water level. The average concentration at all stations of DSi, PSi, and phosphate were 182.3 ± 38.0, 156.1 ± 72.5, and 1.5 ± 1.1 μmol L^{-1}, respectively. The DSi, PSi, and phosphate concentrations at station A25 during ordinary water level were 220.9 ± 27.7, 18.2 ± 16.1, and 11.9 ± 5.6 μmol L^{-1}, respectively. The DSi concentration during the flooding event was slightly lower than that during ordinary water level; the phosphate concentration was two to seven times lower than that during ordinary water level. In contrast, the PSi concentration during the flooding events was about 16 times higher than that during ordinary water level. The DSi and phosphate concentrations were almost the same as in the middle river during ordinary water level. In other rivers, the DSi concentrations during flooding events were also lower than that during ordinary water level (Zhang et al., 2009; Herbeck et al., 2011; Chen et al., 2018; Su et al., 2018). The DSi concentration of rainwater was very low (Sferratore et al., 2006). In addition, the DSi concentration of rainwater collected at the Arakawa river basin of upper stream water was lower than the detection limit. This means that DSi was diluted by the rain, leading to a decrease in its concentrations. Su et al. (2018) reported that the release of DSi solute-rich soil waters could induce a greater contribution to the loading amount during storm events rather than silicate bedrock weathering. Therefore, flooding events promoted DSi rich soil water export from the basin because dilution derived from rainwater was low.

The loading amount of DSi was 1.2×10^8 ($\pm 0.1 \times 10^8$) mol $15days^{-1}$ during flooding events (15 days from October 12, 2019 to October 26, 2019). It was equivalent to the annual DSi loading during ordinary water level, which was 1.5×10^8 ($\pm 0.1 \times 10^8$) mol $year^{-1}$ (365 days from October 1, 2018 to September 30, 2019). The loading amount of PSi was 0.15×10^8 ($\pm 0.02 \times 10^8$) mol $year^{-1}$ during ordinary water level and was 2.4×10^8 ($\pm 0.4 \times 10^8$) mol $15days^{-1}$ during flooding events, which was about 16 times higher. As a result, the load of silicon was 1.7×10^8 ($\pm 0.1 \times 10^8$) mol $year^{-1}$ during ordinary water level and it increased by two times during flooding events to 3.6×10^8 ($\pm 0.4 \times 10^8$) mol $15days^{-1}$. During ordinary water level, the ratio of PSi to the total amount of silicon load was about 9.1%, but at the time of flooding, it was about 67%. The amount of estimated phosphate load was 6.0×10^6 ($\pm 1.7 \times 10^8$) mol $year^{-1}$ during ordinary water level and was 2.0×10^6 ($\pm 0.4 \times 10^8$) mol $15days^{-1}$ during flooding events, which was about 30% of annual loading. During the ordinary water level period from October 1, 2018 to September 30, 2019, there were a few flooding events due to the Typhoon. However, the effects of these typhoons were very small because the precipitation was about 30 to 60 mm. Therefore, higher amounts of silicon and phosphate, which were estimated in previous studies, may be supplied to the estuary during large-scale flooding events.

Conclusion

The concentrations of DSi and PSi were measured at Arakawa River from upper stream to downstream throughout the year included flooding event. The large increase in DSi concentrations in the middle river was due to inflow of STP effluents throughout the year. In addition, the ratio of DSi/phosphate was greatly reduced in the downstream due to input of low DSi/phosphate water from STPs. During flooding events for 15 days, loading amounts of DSi and PSi were 80% and 1600% compared to annual loadings during ordinary water level, which were excluded flooding events. Tropical storms are largely associated with material export from the land to the ocean (Thomas, 1994; Kao and Milliman, 2008; Kao et al., 2010; Milliman and Farnsworth, 2011; Lévyetal, 2012; Menkesetal, 2016). In the coming years, extreme weather due to climate change and heavy rainfall due to typhoons is expected to increase (Staten et al., 2018; Yamaguchi et al., 2020). Therefore, it is necessary to continuously accumulate data on mass transport during large-scale flooding events and to estimate changes in the material cycle in coastal waters in the future.

Acknowledgement

We thank Ms. Chinatsu Ouchida-Kubo for her help in sampling. This work was supported by Early-Career Scientist (19K20436) from the Ministry of Education, Culture, Sports, Science, and Technology, Japan.

References

Beale, B. M. L., 1962, Some uses of computers in operational research. Industrielle Organisation, 31, 27-28.

Becker, S., Aoyama, M., Woodward, E. M. S., Bakker, K., Coverly, S., Mahaffey, C., and Tanhua, T., 2019, GO-SHIP Repeat Hydrography Nutrient Manual: The precise and accurate determination of dissolved inorganic nutrients in seawater, using Continuous Flow Analysis methods. Scientific Committee on Oceanic Research, 1-56.

Bindoff, N. L., Cheung, W. W. L., Kairo, J. G., Arístegui, J., Guinder, V. A., Hallberg, R., Hilmi, N., Jiao, N., Karim, M. S., Levin, L., O’Donoghue, S., Purca Cuicapusa, S. R., Rinkevich, B., Suga, T., Tagliabue, A., and Williamson, P., in press, Changing Ocean, Marine Ecosystems, and Dependent Communities. In: Pörtner, H. O., Roberts, D. C., Masson-Delmotte, V., Zhai, P., Tignor, M., Poloczanska, E., Mintenbeck, K., Alegría, A., Nicolai, M., Okem, A., Petzold, J., Rama, B., Weyer, N. M., (eds.), IPCC Special Report on the Ocean and Cryosphere in a Changing Climate.

Chauvin, F., Pilon, R., Palany, P., and Belmadanl, A., 2020, Future changes in Atlantic hurricanes with the rotated-stretched ARPEGE-Climat at very high resolution. Climate Dynamics, 54, 947-972.

Chen, N., Kron., M. D., Wu, Y., Yu, D., and Hong, H., 2018, Storm induced estuarine turbidity maxima and controls on nutrient fluxes across river-estuary-coast continuum. Science of the Total Environment, 628-629, 1108-1120.

Dolan, D. M., Yui, A. K., Geist, R. D., 1981, Evaluation of river load estimation methods for total phosphorus. Journal of Great Lakes Research, 7, 207-214.

Fulweiler, R. W., and Nixon, S. W., 2005, Terrestrial vegetation and the seasonal cycle of dissolved silica in a southern New England coastal river. Biogeochemistry, 74, 115-130.

Furumai, H., 2008, Rainwater and reclaimed wastewater for sustainable urban water use. Physics and Chemistry of the Earth, 33, 340-346.

Furumai, H., Yamamoto, K., and Sato, K., 2012, Silicic Acid, source and whereabouts, Gihoudo Tokyo, 181pp (in Japanese).

Herbeck, L. S., Unger, D., Krumme, U., Liu, S. M., and Jennerjahn, T. C., 2011, Typhoon-induced precipitation impact on nutrient and suspended matter dynamics of a tropical estuary affected by human activities in Haian, China. Estuarine, Coastal and Shelf Science, 93, 375-388.

Hansen, H. P., and Koroleff, F. 1999. Determination of nutrients, p. 159–227. In Grasshoff, K., Kremling, K., and Ehrhardt, M. (eds.), Methods of seawater analysis. Wiley-VCH.

Hashihama, F. 2018. Biogenic Silica, p. G402JP:001–004. In Ono, T. (ed), Guideline of ocean observations, The Oceanographic Society of Japan, ISBN 978-4-908553-42-4 (in Japanese).

Inoue, N., and Akagi, T., 2006, The influence of the dam and sewage treatment plants of the silicon budget of the Tamagawa River. Chikyukagaku (Geochemistry), 40, 137-145 (in Japanese with English abstract).

Kao, S. J., Dai, M., Selvaraj, K., Zhai, W., Cai, P., and Chen, S. N., 2010, Cyclone-drive deep sea injection of freshwater and heat by hyperpycnal flow in the subtropics. Geophysical Research Letters, 37, L21702.

Kao, S. J., and Milliman, J. D., 2008, Water and sediment discharges from small mountainous rivers, Taiwan: The roles of lithology, episodic events, and human activities. Journal of Geology, 116, 431–448.

Krausse, G. L., Schelske, C. L., and Davis, C. O., 1983, Comparison of three wet-alkaline methods of digestion of biogenic silica in water. Freshwater Biology, 13, 73-81.

Kubo, A., Hashihama, F., Kanda, J., Horimoto-Miyazaki, N., and Ishimaru, T., 2019, Long-term variability of nutrient and dissolved organic matter concentrations in Tokyo Bay between 1989 and 2015. Limnology and Oceanography, 64, S202-S222.

Kubo, A., Maeda, Y., and Kanda, J., A significant net sink for CO_2 in Tokyo Bay. Scientific Reports, 7, 44355, doi: 10.1038/srep44355.

Kubo, A., Yamamoto-Kawai, M., and Kanda, J., 2015, Seasonal variations in concentration and lability of dissolved organic carbon in Tokyo Bay. Biogeosciences, 12, 269-279.

Kumagai, H., Tanaka, Y., Ishibashi, Y., and Matsuo, H., Survey of dissolved silicate in industrial effluents from specified facilities, Journal of Japan Society on Water Environment, 2011, 34, 11-17.

Lévy, M., Lengaigne, M., Bopp, L., Vincent, E. M., Madec, G., and Ethé, C., 2012, Contribution of tropical cyclones to the air-sea CO2 flux: A global view. Global Biogeochemical Cycles, 26, GB2001.

Maavara, T., Chen, Q., van Meter, K., Brown, L. E., Zhang, J., Ni, J., and Zarfl, C., 2020, River dam impacts on biogeochemical cycling. Nature Review, 1, 103-116.

MacDonald, R.W., McLaughlin, F.A., and Wong, C.S. 1986. Storage of reactive silicate samples by freezing. Limnology and Oceanography, 31, 1139-1142.

Maguire, T. J., and Fulweiler, R. W., 2017, Fate and Effect of Dissolved Silicon within Wastewater Treatment Effluent. Environmental Science and Technology, 51, 7403-7411.

Menkes, C. E., Lengaigne, M., Lévy, M., Ethé, C., Bopp, L., and Aumont, O., 2016, Global impact of tropical cyclones on primary production. Global Biogeochemical Cycles, 30, 767–786.

Milliman, J. D., and Farnsworth, K. L., 2011, River discharge to the coastal ocean: A global synthesis, 384, Cambridge University Press.

Miyashita, Y. 2004, Relation between quality of nitrate nitrogen pollution groundwater, stable isotope of nitrogen, and land use in Kanagawa Prefecture, Bulletin of the Hot Springs Research Institute of Kanagawa Prefecture, 36, 25-44 (in Japanese with English abstract).

Murphy, J., and J. P. Riley. 1962. A modified single solution method for the determination of phosphate in natural. Analytica Chimica Acta 27: 31–36. doi:10.1016/S0003-

2670(00)88444-5

Nelson, D. M., Tréguer, P., Brzezinski, M. A., Leynaert, A., and Queguiner, B., 1995, Production and dissolution of biogenic silica in the ocean: Revised global estimates, comparison with regional data and relationship to biogenic sedimentation. Global Biogeochemical Cycles, 9, 359–372.

Nihei, Y., Ehara, M., Usuda, M., Sakai, A., and Shigeta, K., 2007, Water quality and pollutant load in the Edo River, Ara River, and Tama River. Coastal Engineering Journal, 54, 1226-1230 (in Japanese with English abstract).

Ragueneau, O., and Tréguer, P., 1994, Determination of biogenic silica in coastal waters: applicability and limits of the alkaline digestion method. Marine Chemistry, 45, 43-51.

Ragueneau, Conley, D. J., Leynaert, A., Longphuirt, S. N., and Slomp, C. P., 2006, Role of diatoms in silicon cycling and coastal marine food webs, p. 163–195. In Ittekkot, V., Unger, D., Humborg, C., and An, N. T. (eds.), The Silicon Cycle. Island Press.

Richards, R.P., 1999, Estimation of pollutant loads in rivers and streams: a guidance document for NPS Programs. Prepared Under Grant X998397–01–0.

Richards, R. P., and Holloway, J., 1987, Monte carlo studies of sampling strategies for estimating tributary loads. Water Resources Research, 23, 1939–1948.

Ricker, W. E., 1973, Linear regressions in fishery research. Board Canada, 30, 409–434.

Rousseaux, C. S., and Gregg, W. W., 2014, Interannual variation in phytoplankton primary production at a global scale. Remote Sensing, 6, 1-19.

Scavia, D., Field, J. C., Boesch, D. F., Buddemeier, R. W., Burkett, V., Cayan, D. R., Fogarty, M., Harwell, M. A., Howarth, R. W., Mason, C., Reed, D. J., Royer, T. C., Sallenger, A. H., and Titus, J. G., 2002, Climate Change Impacts on U. S. Coastal and

Marine Ecosystems. Estuaries, 25, 149-164.

Sferratore, A., Garnier, J., Billen, G., Conley, D. J., and Pinault, S., 2006, Diffuse and point sources of silica in the Seine River Watershed. Environmental Science and Technology, 40, 6630-6635.

Suzuki, R., and Ishimaru, T., 1990, An improved method for the determination of phytoplankton chlorophyll using N, N-dimethylformamide. Journal of Oceanography Society of Japan, 46, 190-194.

Staten, P. W., Lu, J., Grise, K. M., Davis, S. M., and Birner, T., 2018, Re-examining tropical expansion. Nature Climate Change, 8, 768-775.

Su, N., Yang, S., and Xie, X., 2018, Typhoon-enhanced silicon and nitrogen exports in a mountainous catchment. Journal of Geophysical Research. Biogeosciences, 123, 2270-2286.

Tanaka, Y., Nagai, N., Suzuki, K., Shimizu, K., 2007, Study of characteristics of residual currents at Daini-Kaiho in Tokyo Bay using the NOWPHAS observation data. Technical Note of the Port and Airport Research Institute, No. 1168 (in Japanese with English abstract).

Thomas, M. F., 1994, Geomorphology in the tropics: A study of weathering and denudation in low latitudes. New York: Wiley.

Touma, D., Stevenson, S., Camargo, S. J., Horton, D.E., and Diffenbaugh, N. S., 2019, Variations in the intensity and spatial extent of tropical cyclone precipitation. Geophysical Research Letters, 46, 13992-14002.

Tréguer, P., and De La Rocha, C, L., 2013, The world ocean silica cycle. Annual Review of Marine Science, 5, 477-501.

Van Dokkum, H. P., Hulskotte, J. H. J., Kramer, K. J. M., and Wilmot, J., 2004, Emission, fate and effects of soluble silicates (waterglass) in the aquatic environment. Environmental Science and Technology, 38(2), 515-521.

Wei, Q., Yao, Q., Wang, B., Wang, H., and Yu, Z., 2015, Long-term variation of nutrients in the southern Yellow Sea. Continental Shelf Research, 111, 184-196.

Yamaguchi, M., Chan, J. C. L., Moon, I., Yoshida, K., and Mizuta, R., 2020, Global warming changes tropical cyclone translation speed. Nature Communications, 10, 1-7.

Yang, F., Wei, Q., Chen, H., and Yao, Q., 2018, Long-term variations and influence factors of nutrients in the western North Yellow Sea, China. Marine Pollution Bulletin, 135, 1026-1034.

Zhang, J-Z., Kelble, C. R., Fischer, C. J., and Moore, L., 2009, Hurricane Katrina induced nutrient runoff from an agricultural area to coastal waters in Biscayne Bay, Florida. Estuarine, Coastal and Shelf Science, 84, 209-218.

Zhang, J-Z., and Ortner, P. B., 1998, Effect of thawing condition on the recovery of reactive silicic acid from frozen natural water samples. Water Research, 32, 2253-2255.

Figure 1. Map of the Arakawa River. Locations of sampling points are indicated by black circles.

Figure 2. Seasonal and spatial variations of (a) DSi, (b) PSi, and (c) phosphate concentrations. X-axis indicates the distance from upper stream water. Black circle indicates the data of October 2018, Cross indicates December 2018, white circle indicates February 2019, Black square indicates April 2019, Diamond indicates June 2019, Black square indicates August 2019.

Figure 3. Spatial variations of (a) DSi (black circle) and PSi (cross) concentrations, and (b) phosphate concentrations on October 26, 2019 during the flooding events. X-axis indicates the distance from upper stream water.

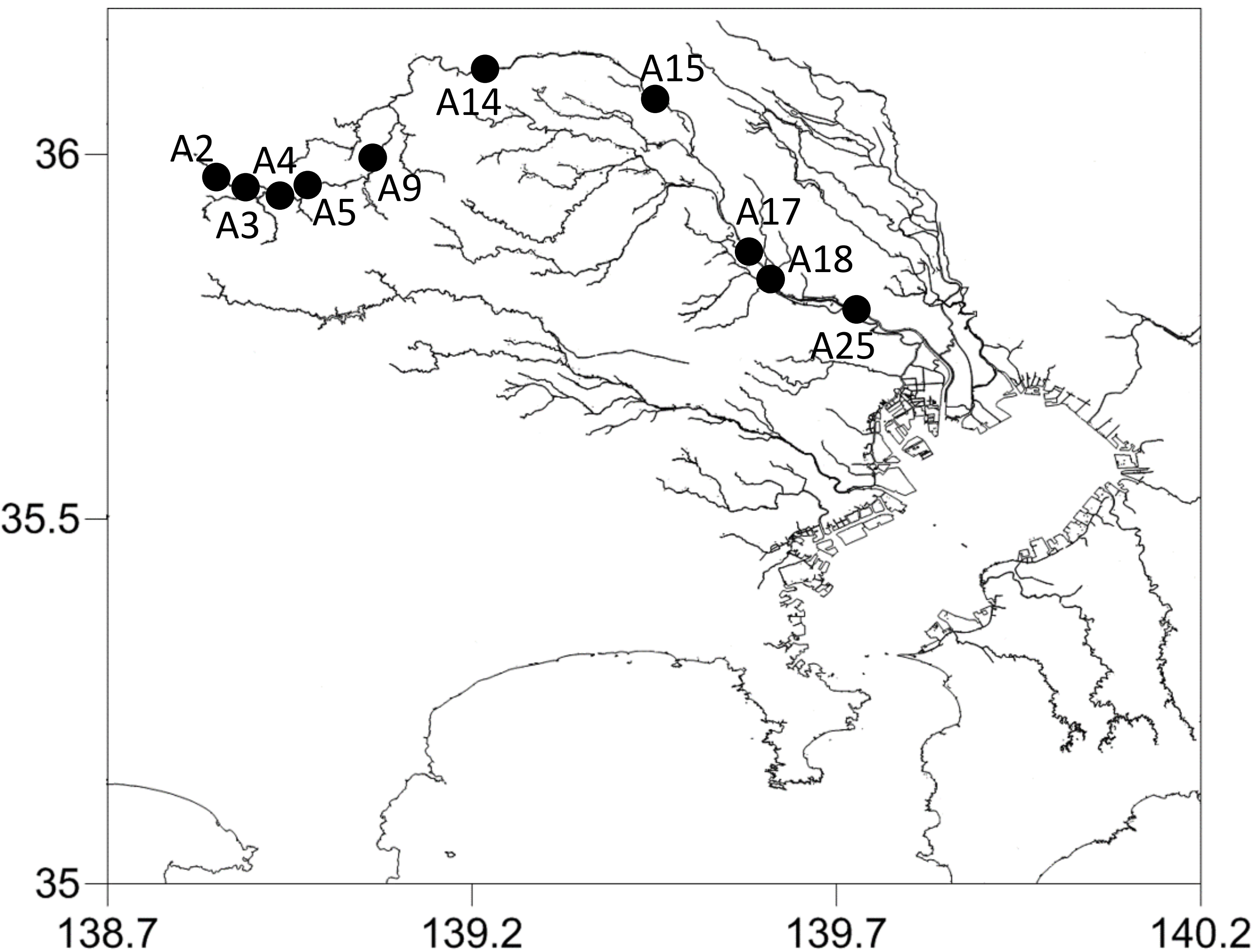

Figure 1

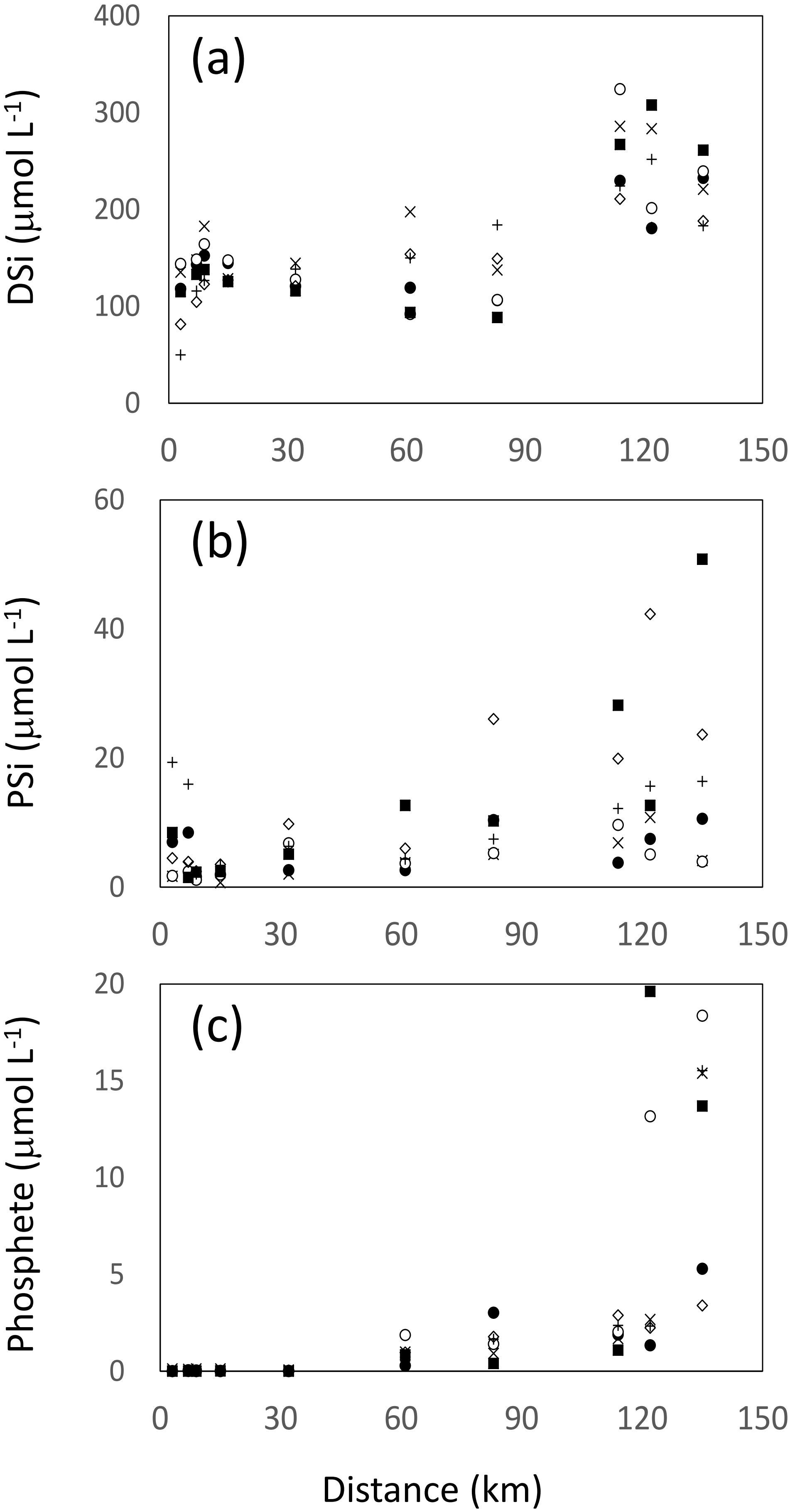
400
300
200
100
0
(a)
DSi (μmol L-1)
0
30
60
90
120
150
60
40
20
0
(b)
PSi (μmol L-1)
20
15
10
5
0
(c)
Phosphete (μmol L-1)
Distance (km)

Figure 2

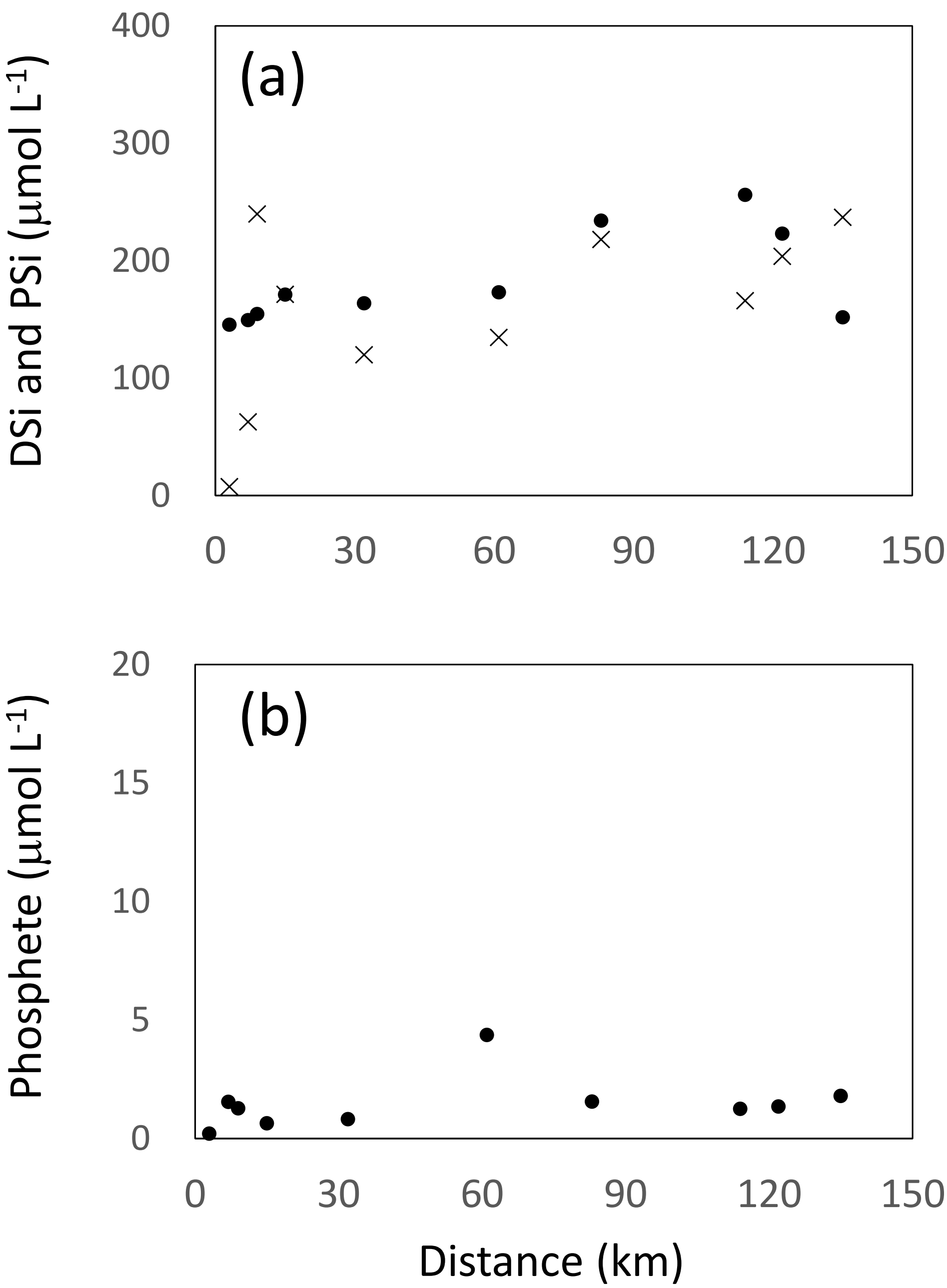

(a)
DSi and PSi (μmol L-1)
400
300
200
100
0
0
30
60
90
120
150
(b)
Phosphete (μmol L-1)
20
15
10
5
0
0
30
60
90
120
150
Distance (km)

Figure 3